Original Article

Interactive effect of hemodynamics in transverse sigmoid sinus and bone morphology on venous pulsatile tinnitus: a four-dimensional (4D) flow magnetic resonance imaging (MRI) study

Ke Lv[1#], Shaowei Zheng[2,3#], Huiying Wang[1], Chenxi Zhao[2], Zhuo Yu[2], Zhiwei Shen[4], Kaixu Xu[5], Chao Chai[6], Shuang Xia[6]

[1]School of Medicine, Nankai University, Tianjin, China; [2]Department of Radiology, First Central Clinical College, Tianjin Medical University, Tianjin, China; [3]Department of Radiology, The First Affiliated Hospital of Dalian Medical University, Dalian, China; [4]Philips Healthcare, Beijing, China; [5]Department of Otolaryngology, Tianjin First Central Hospital, Tianjin, China; [6]Department of Radiology, Medical Imaging Institute of Tianjin, Tianjin First Central Hospital, School of Medicine, Nankai University, Tianjin, China

Contributions: (I) Conception and design: K Lv, S Zheng; (II) Administrative support: K Lv, S Zheng, H Wang, K Xu; (III) Provision of study materials or patients: K Lv, S Zheng, C Zhao; (IV) Collection and assembly of data: K Lv, S Zheng, Z Yu, C Chai; (V) Data analysis and interpretation: K Lv, S Zheng, Z Shen, S Xia; (VI) Manuscript writing: All authors; (VII) Final approval of manuscript: All authors.

[#]These authors contributed equally to this work as co-first authors.

Correspondence to: Shuang Xia, MD; Chao Chai, MD. Department of Radiology, Medical Imaging Institute of Tianjin, Tianjin First Central Hospital, School of Medicine, Nankai University, No. 2 Baoshan West Road, Xiqing District, Tianjin 300192, China. Email: xiashuang77@163.com; chaichao@nankai.edu.cn.

Background: The hemodynamic pathogenesis of venous pulsatile tinnitus (VPT) is still unclear. This study aimed to explore the mechanism of bone morphology and hemodynamic changes in transverse sigmoid sinus (TSS) on VPT patients.

Methods: 49 patients with unilateral VPT, 26 patients with subjective tinnitus and 36 healthy controls were included in this retrospective clinical trial. Four-dimensional (4D) flow magnetic resonance imaging (MRI) was used to evaluate the hemodynamics of the TSS. High-resolution computed tomography was used to assess the perivenous bone structures. All images were independently assessed for each participant by two trained neuroradiologists. Kolmogorov-Smirnov test was used to determine the normal distribution of the data. Chi-square test and nonparametric test were used to compare classified or continuous variables. Stepwise linear regression and mediation effect analysis was used to explore the relationship between bone dehiscence (BD), hemodynamic factors and VPT symptoms.

Results: Peak velocity (P=0.001) and maximum energy loss (P=0.041) in VPT group were risk factors for the severity of tinnitus. Energy loss [indirect effect =0.692, P<0.005, 95% confidence interval (CI): 0.201–1.377] and peak velocity (indirect effect =0.899, P<0.005, 95% CI: 0.406–1.582) demonstrated the complete mediation effect between the BD and VPT. BD showed a complete mediation effect between the wall shear stress (WSS) and VPT (indirect effect =15.181, P<0.005, 95% CI: 3.448–35.493).

Conclusions: Cross-talk between the hemodynamic changes of TSS and BD can regulate the VPT symptoms. This type of analysis might be helpful in establishing the possible occurrence and development mechanism of the hemodynamics and bone morphology of the VPT.

Keywords: Four-dimensional flow magnetic resonance imaging (4D flow MRI); hemodynamics; venous pulsatile tinnitus (VPT); bone morphology; mediation effect analysis

Introduction

Pulsatile tinnitus (PT) is a chronic and rare form of tinnitus with a sensation of hearing rhythmic noise with the same frequency of the heartbeat and pulse (1). PT is caused by vascular abnormalities with venous pulsatile tinnitus (VPT) being a common presentation (2). In recent years, the VPT has been increasingly seen, causing emotional and behavioral impacts, thus affecting the quality of life of people, and some severe cases end up in life-threatening complications (3,4).

Changes in blood flow and bone changes around the sigmoid sinuses are common imaging manifestations of VPT patients. Previous studies on computed tomography (CT) evaluation of the structure found that there were abnormalities in the transverse sigmoid sinus (TSS), such as diverticulum and dehiscence (5-7), resulting in venous pulsations which were captured by the cochlea and produced VPT. Sigmoid sinus bone dehiscence (BD), which is one of the common causes of VPT, can be detected by high-resolution CT (HRCT) (8,9). The VPT is always accompanied by abnormal venous blood flow (10). Some recent studies found that the blood flow in the TSS in patients with VPT was with faster flow velocity, higher flow rate, and presence of turbulence (11-14). However, these observations varied between individuals (11). These analyses were primarily focused on the blood flow volume and velocity (9,13), but a few previous studies focused on the stress parameters acting on the venous wall and perivenous bone, as well as the energy consumption parameters of the blood flow (14). Additionally, further research like mediation effect analysis on the relationship between hemodynamics, bone morphology, and tinnitus occurrence and development is rare.

With the rapid development of three-dimensional (3D) phase contrast magnetic resonance imaging (MRI) technology (15), four-dimensional (4D) flow MRI (when 3D spatial encoding and three-directional time-varying velocity phase contrast MRI are combined) is increasingly used in diagnosing cerebrovascular diseases, such as aneurysms, atherosclerosis, and arteriovenous malformations (16-19). Furthermore, it has been used in VPT research. The 4D flow MRI can simultaneously collect multiple parameters such as velocity, wall shear stress, and energy loss (15). However, the information on the interaction between the abnormal blood flow and BD specific to the severity of VPT is presently lacking. Therefore, we aimed to comprehensively elucidate the location of abnormal blood flow in VPT patients using 4D flow MRI. Additionally, we planned to determine the risk factors contributing to VPT. Subsequently, the interaction between hemodynamic changes of TSS detected by 4D flow MRI and BD detected by HRCT will be investigated, their contributions to the severity of VPT will also be studied using the mediation effect analysis. We present this article in accordance with the STROBE reporting checklist (available at https://qims.amegroups.com/article/view/10.21037/qims-24-610/rc).

Methods

The retrospective study was conducted in accordance with the Declaration of Helsinki (as revised in 2013). The study was approved by institutional ethics board of Tianjin First Central Hospital (No. 2017N002KY) and individual consent for this retrospective analysis was waived.

Participants

Forty-nine patients with clinically confirmed unilateral VPT were included in this study and the VPT was diagnosed according to the criteria from the previous studies (10,13). They were as follows: (I) patients who had rhythmic sounds consistent with the heartbeat, which were relieved or absent when the internal jugular vein was compressed on the side of symptoms; (II) otoscopy and imaging examination excluded other causes such as glomus tympanicum tumors and glomus jugular tumors that could have caused PT. Twenty-six patients with clinically confirmed non-pulsatile subjective tinnitus were included in the subjective tinnitus (ST) group and 36 healthy controls without tinnitus symptoms were included in the healthy controls (HCs) group. The diagnostic criteria of the ST are in the Appendix 1. The clinical characteristics of the subjects were gender, age, side of the symptoms, duration of disease, body mass index (BMI), and presence of dominant drainage (DD) in the transverse-sigmoid sinus and high jugular bulb (HJB), and

the diagnostic criteria can be seen in Figure S1 (17,18).

Assessment of tinnitus severity

Tinnitus Handicap Inventory (THI) was used to assess the severity of tinnitus in VPT and ST patients. It is a comprehensive scale and can simultaneously assess the function, mood, and patients' response to symptoms, with high internal consistencies (19). The scale consisted of 25 questions with a full score of 100, and a higher score indicated that the tinnitus was more severe.

Imaging protocol

The HRCT on the temporal bone was carried out using a Somatom force CT scanner (Siemens Healthineers, Marburg, Germany). The parameters used for scanning were slice thickness of 0.75 mm and tube current of 150 mAs and tube voltage of 120 kVp per slice. The MRI was performed on all subjects using a 3.0T magnetic resonance scanner (Philips Ingenia, 3.0T, Amsterdam, the Netherlands) and 4D flow MRI data were acquired using a free-breathing, peripheral pulse-gated, and multi-shot turbo field echo sequence (Appendix 1), with 3-direction velocity encoding on a 4-point velocity encoding scheme. The velocity encoding was set to 75 cm/s in all directions. The phase-encoding steps per segment resulted in a temporal resolution of 49–51 ms, which was interpolated to 14–16 cardiac phases per cardiac cycle. The 3D-PC-MRV scan was also performed in this study.

Imaging analysis

The HRCT and MR images were independently assessed for each patient by two trained neuroradiologists with 2 and 8 years of neuroradiological experience, respectively, who were blinded to the clinical information of all subjects. The standard HRCT images were carefully evaluated to ensure that all transverse sigmoid dehiscence could be found. The two neuroradiologists determined the presence of dehiscence and subsequently counted the amount of dehiscence. After multiple plane reconstruction of HRCT, the maximum diameter of each fissure was measured. If a patient had multiple defects, the sum of the maximum diameter line of each defect represented the diameter of the BD in a patient (*Figure 1*).

Hemodynamic analysis

The commercially available software CVI-42 (Circle Cardiovascular Imaging, Inc., Calgary, AB, Canada) was used for post-processing analysis of the hemodynamic 4D flow MRI data from all subjects (20). Post-processing methods were reported in the consensus recommendations (21) and a previous study (22). The specific measurement process is shown in *Figure 1* and Appendix 1.

Six measurement planes were set to assess the hemodynamics of each subject. When setting the free planes, we ensured the same position of the measurement plane setting using the three-dimensional display function per subject, and it also should be noted that the plane was set in the direction perpendicular to the blood flow. All vessels were included based on the following criteria: (I) vessels were clear enough for the accurate measurement, (II) no vascular malformations or arteriovenous fistulas significantly affected the hemodynamics. Since all patients with VPT included in our study had unilateral tinnitus, we performed unilateral measurements each time. For subjects in the ST group, we included the vessels on the symptomatic side. For the HCs, we included the bilateral vessels if they met the above criteria.

The following hemodynamic parameters selected for the analysis were total blood flow volume (TV) (mL); peak velocity (PV) (cm/s); maximum wall shear stress (MWSS) (Pa); in all six planes and maximum energy loss (MEL) (mW) between plane 1 and plane 6. The calculation method for wall shear stress (WSS) was reported in a previous study (14). In 4D flow MRI, WSS could be calculated from two-dimensional (3D) analysis planes perpendicular to the vascular lumen or, as more recently demonstrated, by 3D techniques. Images were corrected for background offset errors and velocity aliasing artifacts. WSS represented the tangential force displayed by a layer of fluid on the endothelial surface, mathematically defined as the product of shear rate and shear stress (23). The calculation formula for WSS was as follows:

$$\bar{\tau} = 2\mu \begin{bmatrix} \dfrac{\partial v_x}{\partial x} & \dfrac{1}{2}\left(\dfrac{\partial v_y}{\partial x}+\dfrac{\partial v_y}{\partial y}\right) & \dfrac{1}{2}\left(\dfrac{\partial v_z}{\partial x}+\dfrac{\partial v_x}{\partial z}\right) \\ \dfrac{1}{2}\left(\dfrac{\partial v_x}{\partial y}+\dfrac{\partial v_y}{\partial x}\right) & \dfrac{\partial v_y}{\partial y} & \dfrac{1}{2}\left(\dfrac{\partial v_z}{\partial y}+\dfrac{\partial v_y}{\partial z}\right) \\ \dfrac{1}{2}\left(\dfrac{\partial v_x}{\partial z}+\dfrac{\partial v_z}{\partial x}\right) & \dfrac{1}{2}\left(\dfrac{\partial v_y}{\partial z}+\dfrac{\partial v_z}{\partial y}\right) & \dfrac{\partial v_z}{\partial z} \end{bmatrix} \bar{n} \quad [1]$$

6650

Lv et al. Interaction between hemodynamics and bone morphology on VPT
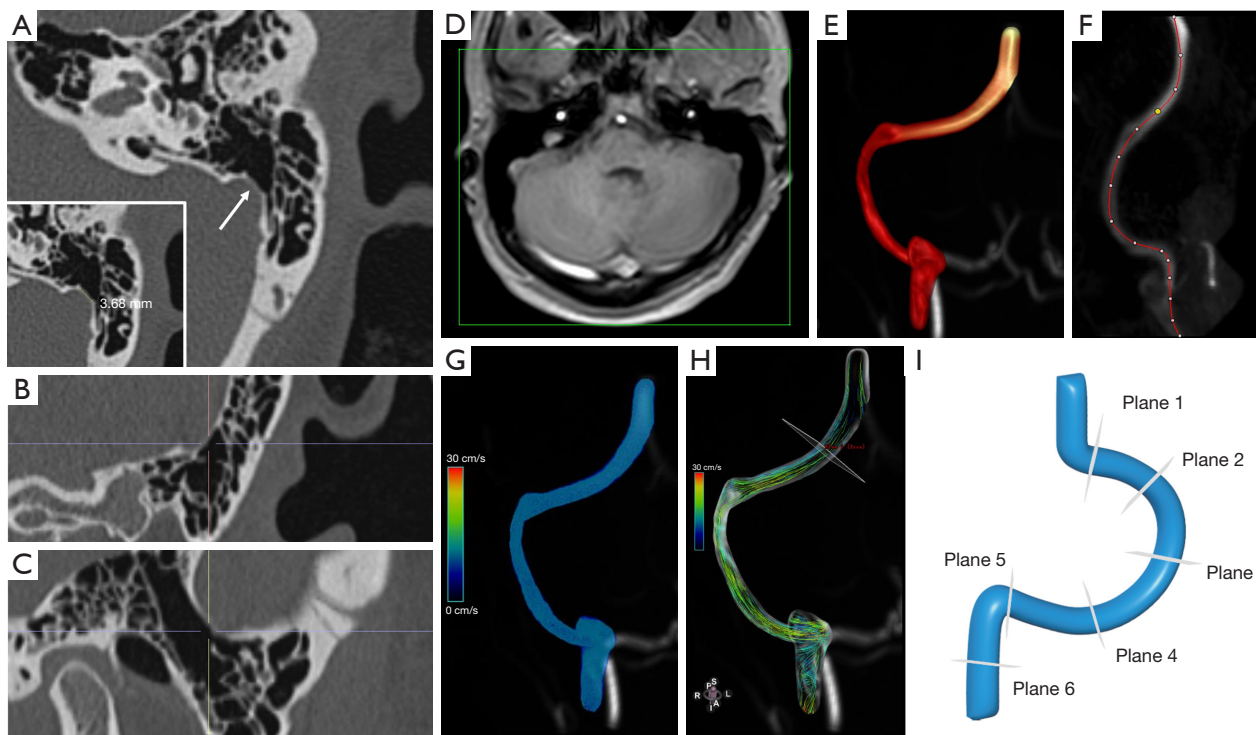
Figure 1 Schematic diagram of the bone defect and hemodynamic measurement. (A) The measurement of maximum diameter of sigmoid sinus' dehiscence. (B,C) Multiple plane reconstruction technology was used to find the plane with the largest range of dehiscence for measurement. (D-I) Hemodynamic measurement steps and the measurement planes. (D) Manually outlined region of interests. (E) Manually segmented vessels of interest. (F) The tracked centerline of the vessels of interest. (G) The vessels of interest that were analyzed and calculated. (H) The observed streamline and placed free plane. (I) The six measurement planes.

Energy loss (EL) was calculated within a predefined segmentation from sinus confluence to internal jugular vein. Peak systolic and average EL per cardiac cycle were sampled per considered tract. Barker *et al.* (24) theoretically deduced and described the EL dissipation caused by viscous energy loss, in which the viscous dissipation was calculated by the viscous component of the Navier Stokes flow energy equation of incompressible fluid according to a single prime basis in a predefined region of interest. The centerline through our vascular segmentation of interest helped depict EL within a predetermined volume range (25). The calculation formula for EL was as follows (14):

$$\Phi_V = \frac{1}{2}\sum_i \sum_j \left[\left(\frac{\partial v_i}{\partial x_j} + \frac{\partial v_j}{\partial x_j} - \frac{2}{3}(\nabla \cdot v)\delta_{ij} \right) \right]^2 \quad [2]$$

where $\delta_{ij} = 1$ for $i = j$ and $\delta_{ij} = 0$ for $i \neq j$

$$EL = \mu \sum_{i=1}^{\text{num voxels}} \Phi_v V_i \quad [3]$$

Statistical analysis

Statistical analysis was performed using SPSS version 25.0 (IBM Corp., Armonk, NY, USA). The Kolmogorov-Smirnov test was used to determine the normal distribution of the data. The categorical data were expressed as the frequency with percentages. The continuous data were presented as median and interquartile range (IQR) (the range between the 25th and 75th percentiles). The Chi-square test was used to compare the differences of the categorical variables including gender, side of symptoms, DD, and HJB. The nonparametric test was used to compare continuous variables including BMI, PT duration, THI score, and hemodynamic parameters. Stepwise linear regression analysis was employed to explore the risk factors of the BD and the severity of the VPT. Mediation effect analysis was performed to explore the relationship between hemodynamic factors, BD, and PT severity. The P value of <0.05 was considered statistically significant.

Table 1 Demographic characteristics of the study sample

Demographic characteristics	VPT group (n=49)	ST group (n=26)	HCs group (n=36)	Statistical value	P value
Age (years)	38±9	40±11	39±11	3.514	0.103
Gender (female)				11.437	0.003[†]
M	8 (16.3)	14 (53.8)	12 (33.3)		
F	41 (83.7)	12 (46.2)	24 (66.7)		
BMI (kg/m^2)	24.0±2.7	23.1±2.5	23.1±2.8	2.123	0.346
HJB				16.060	0.013[†]
No	15 (30.6)	12 (46.2)	25 (69.4)		
Ipsilateral L	13 (26.5)	2 (7.7)	3 (8.3)		
Ipsilateral R	16 (32.7)	8 (30.8)	6 (16.7)		
Bilateral	5 (10.2)	4 (15.4)	2 (5.6)		
DD				5.283	0.259
No	20 (40.8)	12 (46.2)	20 (55.6)		
Ipsilateral L	9 (19.4)	3 (11.5)	1 (2.8)		
Ipsilateral R	20 (40.8)	11 (42.3)	15 (41.7)		

Data are represented as mean ± standard deviation or number (%). [†], P<0.05. VPT, venous pulsatile tinnitus; ST, non-pulsatile subjective tinnitus; HCs, healthy controls; M, male; F, female; BMI, body mass index; HJB, high jugular bulb; L, left; R, right; DD, side of dominant drainage.

Results

Demographics

Demographic and clinical characteristics of all participants are shown in the *Table 1*. The study included 49 patients (49 veins) with clinically confirmed unilateral VPT. In the control groups, 26 ST patients (32 veins) and 36 HCs (51 veins) were included. The majority of patients with VPT were young and middle-aged (mean age, 38±9 years) with a predilection of female (41/49, 83.7%). Compared with the ST group (53.8%) and HCs group (30.6%), the patients in the VPT group often had HJB (69.4%) with a P value of 0.013.

In the VPT group, the median duration of symptoms was 32 [12–96] weeks. Twenty-seven patients with VPT had tinnitus symptoms on the right side. The median THI scores were 40 [31–52] points. Forty-two (85.7%) patients showed different degrees of BD (5.77, 2.25–12.16 mm). In the ST group, the median duration of symptoms was 49 [11–81] weeks. The median THI score was 28 [20–42] points. No abnormal BD of the sigmoid sinus wall was found in patients with ST (*Table 2*).

Hemodynamic abnormalities in the venous sinus of patients with VPT

There was no significant difference in the TV of the six planes among the three groups, but there were significant differences in the PV and MWSS of the six planes among the three groups (Table S1). The MWSS in plane 2 of the VPT patients was statistically higher than that in other planes, and the PV in plane 3 was statistically higher than that in the other planes (*Figure 2*). Combined with the visual evaluation (*Figure 3*), planes 2 and 3 were identified as segments with abnormal hemodynamics in the VPT patients.

Hemodynamic differences in plane 2 and plane 3 of transverse-sigmoid sinus among the three groups

Compared with the ST group (*Figure 3F-3J*) and HCs group (*Figure 3K-3O*), the venous morphology of patients in the VPT group was more irregular (manifested as uneven signal and irregular shape on the PC-MRV) (*Figure 3A,3B*). Patients with VPT showed faster blood flow velocity (red

6652

Lv et al. Interaction between hemodynamics and bone morphology on VPT

Table 2 Characteristics of symptoms in the venous pulsatile tinnitus patients and subjective tinnitus patients

Characteristics of symptoms	VPT group (n=49)	ST group (n=26)	Statistical value	P value
Median duration of symptom (W)	32 [12–96]	49 [11–81]	−0.201	0.841
Side of symptoms			15.699	
L	22 (44.9)	4 (15.4)		<0.001[‡]
R	27 (55.1)	16 (61.5)		
B	–	6 (23.1)		
THI score	40 [31–52]	28 [20–42]	−1.310	0.190
BD, mm	5.77 [2.25–12.16]			
0	7 (14.3)	–		
1	42 (85.7)	–		

Data are represented as median [interquartile range] or number (%). [‡], P<0.001. VPT, venous pulsatile tinnitus; ST, subjective tinnitus; W, weeks; L, left; R, right; B, bilateral; THI, Tinnitus Handicap Inventory; BD, bone dehiscence.
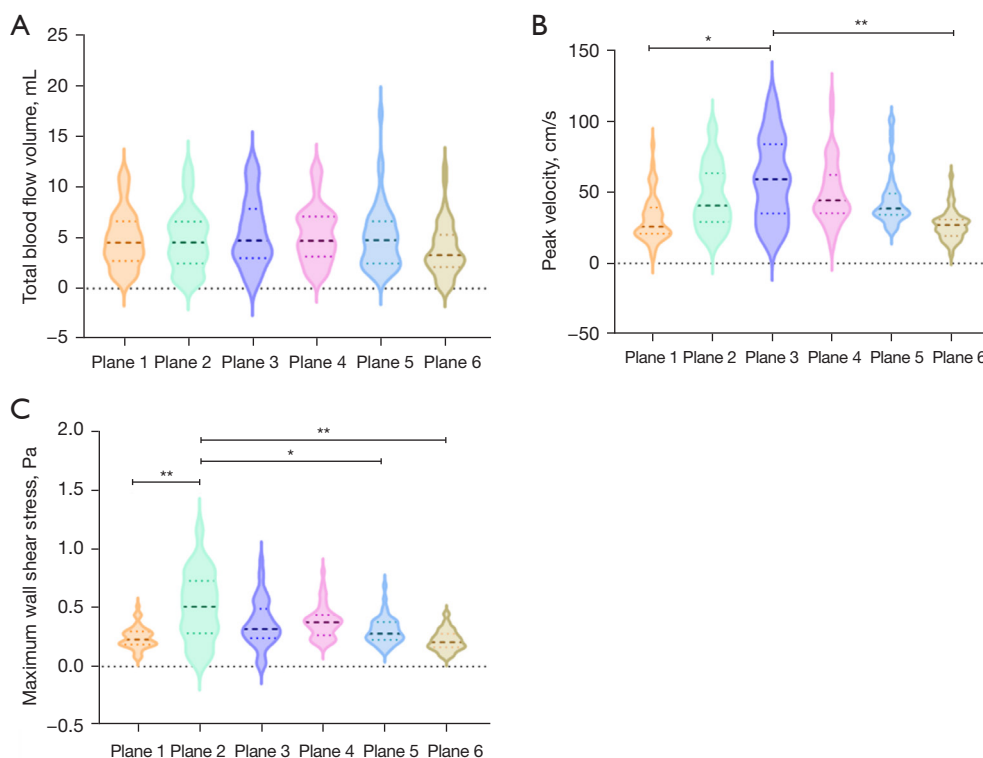
Figure 2 Hemodynamic parameters in the six measurement planes of transverse-sigmoid sinus. Measurement planes with abnormal blood flow in the transverse-sigmoid sinus of patients with VPT were mainly distributed in the middle plane of the transverse sinus to the middle plane of the sigmoid sinus. *, P<0.05; **, P<0.001. VPT, venous pulsatile tinnitus.

streamline in *Figure 3C,3D*) and larger WSS (redder color in *Figure 3E*).

The TV, PV, and MWSS in plane 2 and plane 3 among these three groups, as well as MEL of the whole venous

segment among the three groups, were compared. There was no evidence of a difference in the TV values on these two planes among the three groups. Compared with the ST group and HCs group, the PV on plane 2 and plane 3 in the
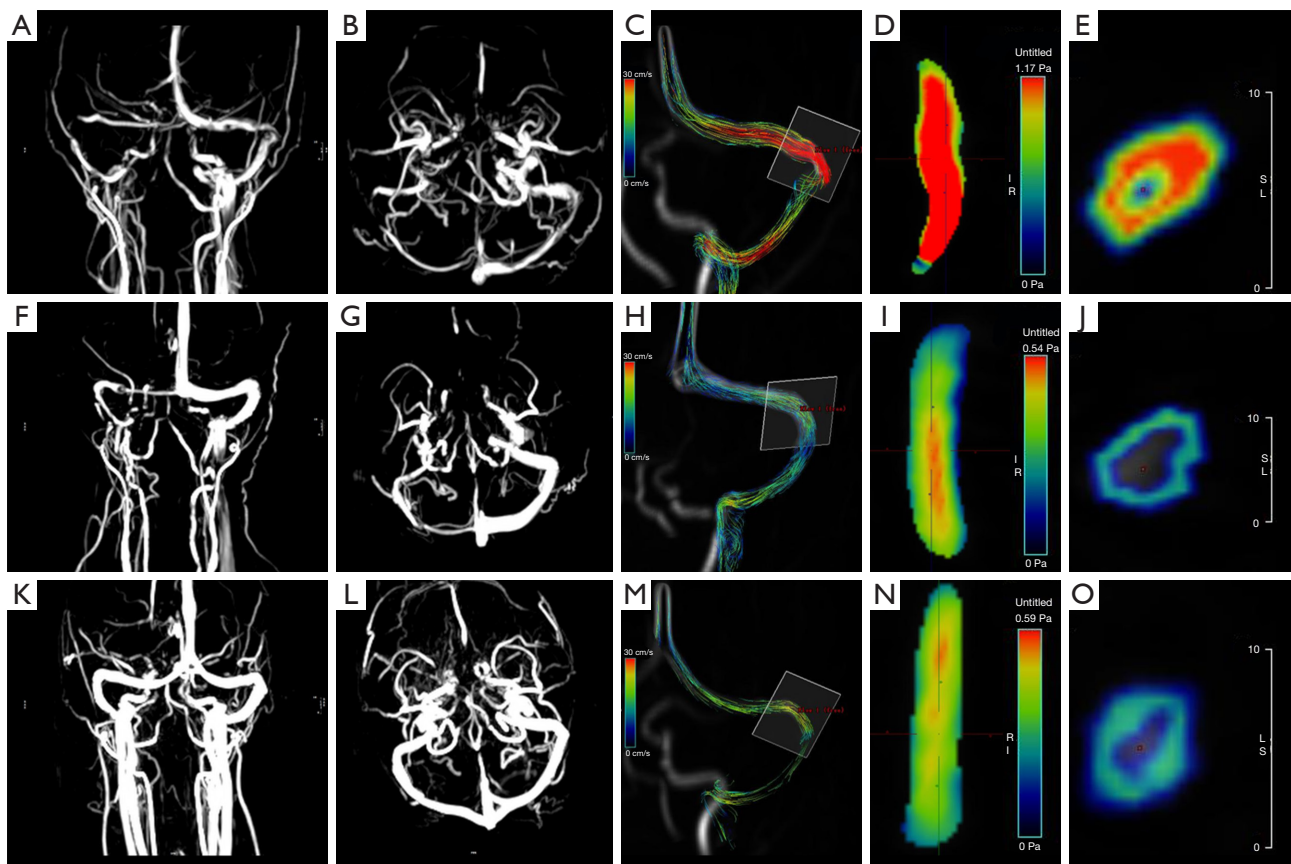
Figure 3 Visualization of 4D flow MRI hemodynamic changes of representative cases among three groups. Compared with the ST patient (F-J) and HCs participant (K-O), the blood flow in the VPT patient (A-E) was more complex. The flow velocity was faster [(C,H,M) shown as the higher flow velocity of the red line, (D,I,N) shown as the higher velocity of red color] and the wall shear stress was greater [(E,J,O) shown as the red pressure area of the cross-section]. 4D, four-dimensional; MRI, magnetic resonance imaging; ST, subjective tinnitus; HCs, healthy controls; VPT, venous pulsatile tinnitus.

patients with VPT was significantly higher, and the MWSS on plane 3 in the patients with VPT was significantly higher. Moreover, the MEL of patients with VPT was also significantly higher than those of the other two groups (*Table 3*, *Figure 4*).

Relationship among hemodynamic factors, BD, and severity of tinnitus

Plane 3 with the largest variability of blood flow was selected as the appropriate measurement plane to explore the relationship between hemodynamic parameters and the BD in patients with VPT. The TV (r=0.313, P=0.028), PV (r=0.620, P<0.001), MWSS (r=0.493, P<0.001), and MEL (r=0.535, P<0.001) were positively related to the size of BD as shown in Figures S2,S3. Additionally, a stepwise

linear regression model was established to explore the hemodynamic risk factors for BD (*Table 4*, Model 1), and found that PV (P=0.003) and MWSS (P=0.018) can be independent risk factors of BD.

THI scale was used to evaluate the severity of tinnitus symptoms in patients with VPT. The TV (r=0.381, P=0.007), PV (r=0.631, P<0.001), MWSS (r=0.367, P=0.010), and MEL (r=0.567, P<0.001) on plane 3 were positively correlated with the THI scores. The size of BD in patients with VPT was also positively correlated with the THI score (r=0.473, P=0.002) (Figures S2,S4).

THI scale was used to evaluate the severity of tinnitus symptoms in patients with ST. Results showed that there were no statistically significant correlation between THI and TV (r=0.320, P=0.074), PV (r=−0.058, P=0.753), MWSS (r=0.009, P=0.960), and MEL (r=−0.108, P=0.556)

6654

Lv et al. Interaction between hemodynamics and bone morphology on VPT

Table 3 Difference of hemodynamics among the three groups

Plane	VPT	ST	HCs	F value	P value
Plane 2					
TV	4.55 (2.47–6.59)	4.15 (2.31–5.61)	4.15 (0.93–5.11)	0.708	0.702
PV	40.68 (29.17–63.48)	29.25 (23.91–34.20)	31.73 (22.44–38.91)	14.614	0.001[†]
MWSS	0.51 (0.28–0.73)	0.43 (0.34–0.53)	0.40 (0.32–0.51)	4.320	0.115
Plane 3					
TV	4.73 (2.99–7.87)	4.50 (2.64–5.56)	3.95 (2.84–5.99)	2.125	0.346
PV	59.27 (35.11–83.91)	28.20 (22.63–34.28)	25.41 (20.78–33.60)	37.044	<0.001[‡]
MWSS	0.32 (0.24–0.49)	0.27 (0.20–0.34)	0.23 (0.19–0.27)	19.046	<0.001[‡]
MEL	1.55 (0.56–5.21)	0.41 (0.29–0.68)	0.67 (0.30–1.20)	26.662	<0.001[‡]

Data are represented as median (25th to 75th). [†], $P<0.05$; [‡], $P<0.001$. VPT, venous pulsatile tinnitus; ST, subjective tinnitus; HCs, healthy controls; TV, total blood flow volume; PV, peak velocity; MWSS, maximum wall shear stress; MEL, maximum energy loss.
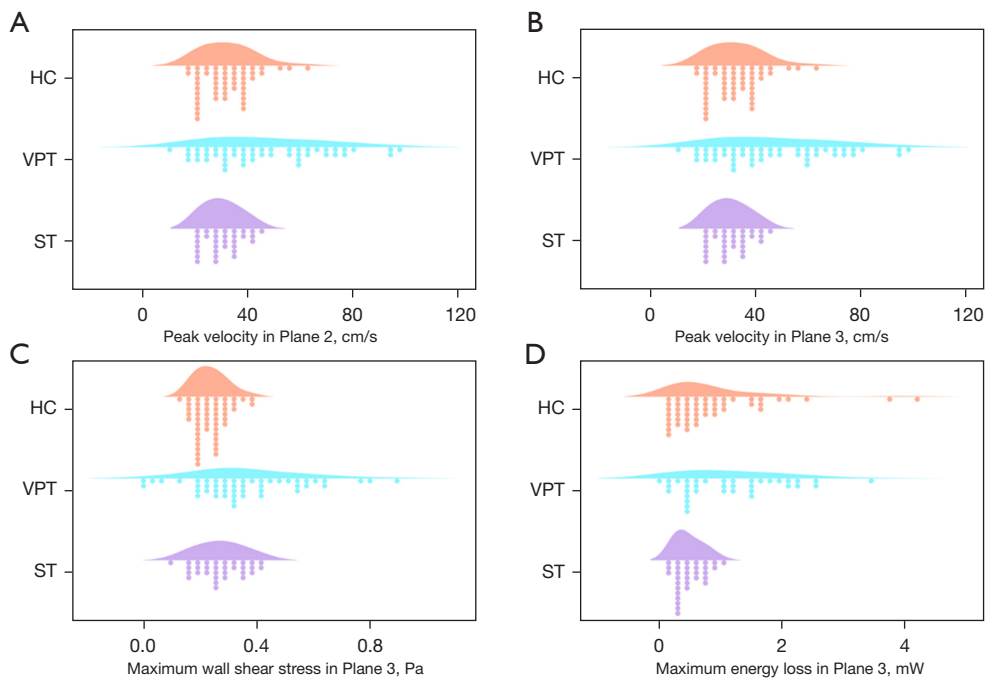

Figure 4 Hemodynamic parameters in the three groups. PV values in Planes 2 (A) and 3 (B) were higher in patients with VPT compared with ST patients and HC participants. MWSS values in Plane 3 were significantly higher in patients with VPT compared with ST patients and HC participants (C). MEL values were significantly higher in the VPT group compared with the ST and HC groups (D). HC, healthy control; VPT, venous pulsatile tinnitus; ST, subjective tinnitus; PV, peak velocity; MWSS, maximum wall shear stress.

on plane 3 in ST group (as shown in Figure S5).

Risk factors of severity of tinnitus in patients with VPT

A stepwise linear regression model was established to evaluate the risk factors of the severity of tinnitus in patients with VPT. Age, duration of symptoms, TV, PV, MWSS, MEL, and BD size were used as independent variables and the THI was used as the dependent variable. The model was statistically significant (F=23.107, P<0.001). The MEL

Table 4 The risk factors of severity of tinnitus using a multiple linear regression

Model	Beta	P value	95% confidence interval		Partial	VIF
			Lower bound	Upper bound		
Bone dehiscence						
PV (cm/s)	0.395	0.003[†]	0.028	0.133	0.367	1.159
MWSS (Pa)	0.315	0.018[†]	1.743	17.424	0.293	1.159
Tinnitus symptom severity						
PV (cm/s)	0.485	0.001[†]	0.124	0.449	0.369	1.731
MEL (mW)	0.298	0.041[†]	0.086	3.743	0.219	1.731

[†], $P<0.05$. VIF, variance inflation factor; PV, peak velocity; MWSS, maximum wall shear stress; MEL, maximum energy loss.

($P=0.041$) and PV ($P=0.001$) were the independent factors for the severity of tinnitus (*Table 4*, Model 2).

The effect of BD on PT severity is mediated by hemodynamic factors

Two sets of mediation effect models were established to explore the relationship among the hemodynamic factors, BD, and VPT severity.

In the first model, the MEL, TV, PV, and MWSS were considered mediation variables, BD was taken as the independent variable, and THI was taken as the dependent variable. MEL [indirect effect =0.692, $P<0.005$, 95% confidence interval (CI): 0.201–1.377] and PV (indirect effect =0.899, $P<0.005$, 95% CI: 0.406–1.582) demonstrated the complete mediation effect between the BD and VPT, as shown in *Figure 5A,5B* and Table S2. However, when the TV and MWSS were used as mediation variables, the model was invalid (Figure S6).

In the second model, BD was considered a mediation variable, the MEL, TV, PV, and MWSS were taken as independent variables, and THI was considered a dependent variable. BD showed a complete mediation effect between the WSS and VPT (indirect effect =15.181, $P<0.005$, 95% CI: 3.448–35.493), as shown in *Figure 5C* and Table S3. However, no significant mediation effect existed between the TV, PV, MEL and THI when the BD was used as a mediation variable (Figure S7).

Discussion

In this study, we focused on the mechanism of occurrence and development of VPT in hemodynamic and bone morphological changes. A detailed analysis of TSS in VPT patients, ST patients, and HC participants was conducted using the 4D flow MRI method. The abnormal blood flow segments of VPT patients were determined, valuable hemodynamic indicators were identified, and further regression analysis and mediation effect analysis were used to determine the impact of hemodynamic indicators and BD on the severity of VPT.

The presence of abnormal flow in patients with VPT at the midpoint of the transverse sinus to the midpoint of the sigmoid sinus was consistent with the presence of abnormalities in the sigmoid sinus wall from previous studies (26,27). This vessel segment was located at the TSS transition, relevant to the congenital physiological curvature (27). Due to the great individual variation in the vein structure, the structure often seems to have some abnormalities. In previous study, transverse sinus stenosis mostly occurred in the lower segment of the transverse sinus (12). Our study further confirmed that the blood flow was more complex, the PV was faster, the WSS was greater, and the EL was greater in patients with VPT when compared with HCs and ST groups. These were consistent with the results of previous studies (10,13). But our study was the first study to observe the changes in WSS and EL in VPT, which further explained the occurrence of VPT from the perspective of mechanics and energy.

Our study confirmed that PV and EL were the risk factors for the severity of VPT. The effect of PV in patients with VPT was evidenced in many previous studies, and similar results were obtained in this study (10-12). The EL was relevant to the kinetic energy consumed by blood as it flowed through a defined vessel. A previous study illustrated the mechanism by which helical features increased the overall energy loss from the system (25). The TSS in our study also exhibited innate morphological curvature and
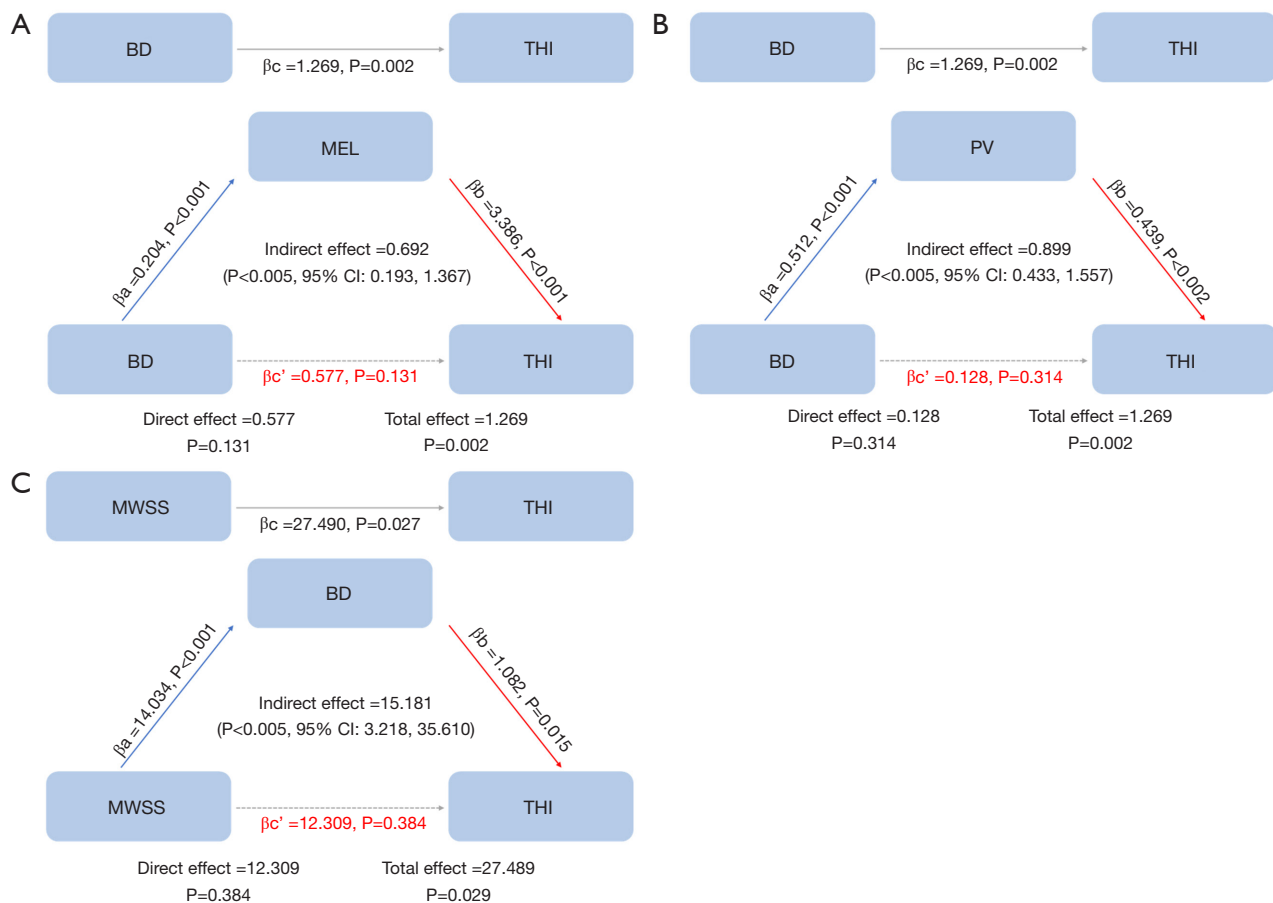
Figure 5 Mediation effect analysis results. The effect of bone dehiscence on the severity of PT mediated by hemodynamic factors (A,B). The MEL (A) and PV (B) mediated the relationship between bone dehiscence and THI. The bone dehiscence (C) exhibited a complete mediation effect between MWSS and THI. BD, bone dehiscence; THI, Tinnitus Handicap Inventory; MEL, maximum energy loss; MWSS, maximum wall shear stress; PV, peak velocity; CI, confidence interval; PT, pulsatile tinnitus.

functional variations (28). Other vascular abnormalities, such as stenosis, vestibule, and abnormal vascular position, were the factors affecting the blood flow trajectory (29,30). The presence of these abnormalities explained why EL was significantly increased in patients with VPT and might have been a risk factor for the severity of tinnitus.

Our study proposed two possible mechanisms of VPT. (I) BD might have caused the abnormal hemodynamic changes, resulting in severe VPT. (II) The abnormal hemodynamic changes might have caused the BD, leading to severe VPT. To explain the first mechanism, all patients with VPT included in this study had BD, and abnormal blood flow was found in the area of BD, indicating that BD may have occurred before the blood flow changes. The abnormality of bone structure led to the increase in blood flow energy consumption and the generation

of flow turbulence (8,31). According to a previous study, not all patients with BD exhibited symptoms of PT (32), but VPT resulted when BD and abnormal blood flow co-occurred. In relevant to the second mechanism, there are studies that suggested BD as one of the risk factors for the occurrence of VPT (32,33). The PV and WSS can affect the intensity of BD. When the blood flows at a higher velocity through the curved blood vessel, the vessel wall bears more pressure to change the direction of the blood flow (32). Elevated WSS can cause the destruction, degradation, and turnover of vascular endothelial cells, increase the production of matrix metalloproteinase by mural cells (33,34), and lead to vascular wall remodeling. With constant pressure, the surrounding bone gradually resorbs and thins, and the protective effect of vasculature is gradually reduced, resulting in BD. Regardless of the

presence of BD, the blood flow changes can produce large pulsating sounds, which can be captured by the cochlea. In addition, relevant studies on surgical treatment like sandwich surgical technique and transient sigmoid sinus decompression surgery of VPT patients also point out that appropriate surgical treatment can effectively alleviate the symptoms and enable patients to achieve a good prognosis (35,36). This also confirms from the perspective of surgical treatment the important impact of hemodynamic and morphological changes on the occurrence and development of VPT.

Our study also had limitations. (I) The number of patients with the presence of the diverticulum was small. Next step will be increasing the sample size and following up timely. (II) Given the area of BD was irregular, our study only measured the maximum diameter of the BD, rather than the area. Although we adopted a strict measurement method, the area should have more accurately reflected the size of BD. (III) There was no golden standard for the *in vivo* EL measurement, but previous hydrodynamics studies found that the results measured by the in vitro mechanical EL were consistent with those measured by the 4D flow MRI. (IV) This study did not focus on the clinical treatment methods and outcomes of VPT patients. (V) Gender, as a nuisance variable, was not analyzed in detail in this study. Further research is needed to explore the mechanism of gender in the onset and progression of VPT in the future.

Conclusions

Complex and aggressive blood flow status causes the pathogenesis of VPT. Abnormal hemodynamic changes can lead to BD and then affect the clinical symptoms of VPT. BD can also reversely cause abnormal hemodynamic changes, further leading to clinical symptoms of VPT and reflecting the possible interactive effect of hemodynamics in TSS and bone morphology on VPT.

Acknowledgments

Footnote

Reporting Checklist: The authors have completed the STROBE reporting checklist. Available at https://qims.amegroups.com/article/view/10.21037/qims-24-610/rc

Conflicts of Interest: All authors have completed the ICMJE uniform disclosure form (available at https://qims.amegroups.com/article/view/10.21037/qims-24-610/coif). Z.S. is an employee of Philips healthcare company. The other authors have no conflicts of interest to declare.

Ethical Statement: The authors are accountable for all aspects of the work in ensuring that questions related to the accuracy or integrity of any part of the work are appropriately investigated and resolved. The retrospective study was conducted in accordance with the Declaration of Helsinki (as revised in 2013). The study was approved by institutional ethics board of Tianjin First Central Hospital (No. 2017N002KY) and individual consent for this retrospective analysis was waived.

References

1. Piccirillo JF, Rodebaugh TL, Lenze EJ. Tinnitus. JAMA 2020;323:1497-8.
2. Bauer CA. Tinnitus. N Engl J Med 2018;378:1224-31.
3. Abdalkader M, Nguyen TN, Norbash AM, Raz E, Shapiro M, Lenck S, Brinjikji W, Weber P, Sakai O. State of the Art: Venous Causes of Pulsatile Tinnitus and Diagnostic

Considerations Guiding Endovascular Therapy. Radiology 2021;300:2-16.

4. Chapel AC, Page JC, Sweeney AD. Hearing Loss, Pulsatile Tinnitus, and Otalgia. JAMA Otolaryngol Head Neck Surg 2021;147:665-6.

5. Kumar R, Rice S, Lingam RK. Detecting causes of pulsatile tinnitus on CT arteriography-venography: A pictorial review. Eur J Radiol 2021;139:109722.

6. Sotoudeh H, Elsayed G, Ghandili S, Shafaat O, Bernstock JD, Chagoya G, Atchley T, Talati P, Segar D, Gupta S, Singhal A. Prevalence of Sigmoid Sinus Dehiscence and Diverticulum among Adults with Skull Base Cephaloceles. AJNR Am J Neuroradiol 2020;41:1251-5.

7. Ettyreddy AR, Shew MA, Durakovic N, Chole RA, Herzog J, Buchman CA, Wick CC. Prevalence, Surgical Management, and Audiologic Impact of Sigmoid Sinus Dehiscence Causing Pulsatile Tinnitus. Otol Neurotol 2021;42:82-91.

8. Lansley JA, Tucker W, Eriksen MR, Riordan-Eva P, Connor SEJ. Sigmoid Sinus Diverticulum, Dehiscence, and Venous Sinus Stenosis: Potential Causes of Pulsatile Tinnitus in Patients with Idiopathic Intracranial Hypertension? AJNR Am J Neuroradiol 2017;38:1783-8.

9. Eisenman DJ, Raghavan P, Hertzano R, Morales R. Evaluation and treatment of pulsatile tinnitus associated with sigmoid sinus wall anomalies. Laryngoscope 2018;128 Suppl 2:S1-S13.

10. Li Y, Chen H, He L, Cao X, Wang X, Chen S, Li R, Yuan C. Hemodynamic assessments of venous pulsatile tinnitus using 4D-flow MRI. Neurology 2018;91:e586-93.

11. Liu Z, He X, Du R, Wang G, Gong S, Wang Z. Hemodynamic Changes in the Sigmoid Sinus of Patients With Pulsatile Tinnitus Induced by Sigmoid Sinus Wall Anomalies. Otol Neurotol 2020;41:e163-7.

12. Han Y, Xia J, Jin L, Qiao A, Su T, Li Z, Xiong J, Wang H, Zhang Z. Computational fluid dynamics study of the effect of transverse sinus stenosis on the blood flow pattern in the ipsilateral superior curve of the sigmoid sinus. Eur Radiol 2021;31:6286-94.

13. Li X, Qiu X, Ding H, Lv H, Zhao P, Yang Z, Gong S, Wang Z. Effects of different morphologic abnormalities on hemodynamics in patients with venous pulsatile tinnitus: A four-dimensional flow magnetic resonance imaging study. J Magn Reson Imaging 2021;53:1744-51.

14. Soulat G, McCarthy P, Markl M. 4D Flow with MRI. Annu Rev Biomed Eng 2020;22:103-26.

15. Morgan AG, Thrippleton MJ, Wardlaw JM, Marshall I. 4D flow MRI for non-invasive measurement of blood flow in the brain: A systematic review. J Cereb Blood Flow Metab 2021;41:206-18.

16. Holmgren M, Wåhlin A, Dunås T, Malm J, Eklund A. Assessment of Cerebral Blood Flow Pulsatility and Cerebral Arterial Compliance With 4D Flow MRI. J Magn Reson Imaging 2020;51:1516-25.

17. Vali A, Aristova M, Vakil P, Abdalla R, Prabhakaran S, Markl M, Ansari SA, Schnell S. Semi-automated analysis of 4D flow MRI to assess the hemodynamic impact of intracranial atherosclerotic disease. Magn Reson Med 2019;82:749-62.

18. Li CQ, Hsiao A, Hattangadi-Gluth J, Handwerker J, Farid N. Early Hemodynamic Response Assessment of Stereotactic Radiosurgery for a Cerebral Arteriovenous Malformation Using 4D Flow MRI. AJNR Am J Neuroradiol 2018;39:678-81.

19. Qureshi AM, Bhatia K, Kostynskyy A, Krings T. Clinical and Angioarchitectural Features of Ruptured Dural Arteriovenous Fistulas. World Neurosurg 2021;147:e476-81.

20. Costello BT, Voskoboinik A, Qadri AM, Rudman M, Thompson MC, Touma F, La Gerche A, Hare JL, Papapostolou S, Kalman JM, Kistler PM, Taylor AJ. Measuring atrial stasis during sinus rhythm in patients with paroxysmal atrial fibrillation using 4 Dimensional flow imaging: 4D flow imaging of atrial stasis. Int J Cardiol 2020;315:45-50.

21. Yoganathan AP, Chandran KB, Sotiropoulos F. Flow in prosthetic heart valves: state-of-the-art and future directions. Ann Biomed Eng 2005;33:1689-94.

22. Bissell MM, Raimondi F, Ait Ali L, Allen BD, Barker AJ, Bolger A, et al. 4D Flow cardiovascular magnetic resonance consensus statement: 2023 update. J Cardiovasc Magn Reson 2023;25:40.

23. Schäfer M, Browne LP, Morgan GJ, Barker AJ, Fonseca B, Ivy DD, Mitchell MB. Reduced proximal aortic compliance and elevated wall shear stress after early repair of tetralogy of Fallot. J Thorac Cardiovasc Surg 2018;156:2239-49.

24. Barker AJ, van Ooij P, Bandi K, Garcia J, Albaghdadi M, McCarthy P, Bonow RO, Carr J, Collins J, Malaisrie SC, Markl M. Viscous energy loss in the presence of abnormal aortic flow. Magn Reson Med 2014;72:620-8.

25. Schäfer M, Ivy DD, Abman SH, Stenmark K, Browne LP, Barker AJ, Mitchell MB, Morgan GJ, Wilson N, Shah A, Kollengode M, Naresh N, Fonseca B, DiMaria M, Buckner JK, Hunter KS, Kheyfets V, Fenster BE, Truong U. Differences in pulmonary arterial flow hemodynamics between children and adults with pulmonary arterial

hypertension as assessed by 4D-flow CMR studies. Am J Physiol Heart Circ Physiol 2019;316:H1091-104.

26. Hofmann E, Behr R, Neumann-Haefelin T, Schwager K. Pulsatile tinnitus: imaging and differential diagnosis. Dtsch Arztebl Int 2013;110:451-8.

27. Van Osch K, Allen D, Gare B, Hudson TJ, Ladak H, Agrawal SK. Morphological analysis of sigmoid sinus anatomy: clinical applications to neurotological surgery. J Otolaryngol Head Neck Surg 2019;48:2.

28. Wenjuan L, Zhaohui L, Ning Z, Pengfei Z, Cheng D, Zhenchang W. Temporal Bone Pneumatization and Pulsatile Tinnitus Caused by Sigmoid Sinus Diverticulum and/or Dehiscence. Biomed Res Int 2015;2015:970613.

29. Bai X, Fu M, Li Z, Gao P, Zhao H, Li R, Sui B. Distribution and regional variation of wall shear stress in the curved middle cerebral artery using four-dimensional flow magnetic resonance imaging. Quant Imaging Med Surg 2022;12:5462-73.

30. Chen W, Song X, Wei H, Fu M, Chen S, Wei C, Zheng Z, Wu J, Li R. Variations of arterial compliance and vascular resistance due to plaque or infarct in a single vascular territory of the middle cerebral artery. Quant Imaging Med Surg 2023;13:7802-13.

31. Essibayi MA, Oushy SH, Lanzino G, Brinjikji W. Venous Causes of Pulsatile Tinnitus: Clinical Presentation, Clinical and Radiographic Evaluation, Pathogenesis, and Endovascular Treatments: A Literature Review. Neurosurgery 2021;89:760-8.

32. Mu Z, Li X, Zhao D, Qiu X, Dai C, Meng X, Huang S, Gao B, Lv H, Li S, Zhao P, Liu Y, Wang Z, Chang Y. Hemodynamics study on the relationship between the sigmoid sinus wall dehiscence and the blood flow pattern of the transverse sinus and sigmoid sinus junction. J Biomech 2022;135:111022.

33. Amans MR, Haraldsson H, Kao E, Kefayati S, Meisel K, Khangura R, Leach J, Jani ND, Faraji F, Ballweber M, Smith W, Saloner D. MR Venous Flow in Sigmoid Sinus Diverticulum. AJNR Am J Neuroradiol 2018;39:2108-13.

34. Kolega J, Gao L, Mandelbaum M, Mocco J, Siddiqui AH, Natarajan SK, Meng H. Cellular and molecular responses of the basilar terminus to hemodynamics during intracranial aneurysm initiation in a rabbit model. J Vasc Res 2011;48:429-42.

35. Sun J, Sun J. Sandwich technique for sigmoid sinus wall reconstruction for treatment of pulsatile tinnitus caused by sigmoid sinus diverticulum/dehiscence. Acta Otolaryngol 2019;139:1063-6.

36. Slater PW, Duhon BH, Feldman DJ. Transtemporal Sigmoid Sinus Decompression: A Novel Surgical Procedure for the Treatment of Idiopathic Pulsatile Tinnitus. Otol Neurotol 2022;43:328-36.

Appendix 1

Materials and methods

Participants

Diagnostic criteria of subjective tinnitus
The diagnostic criteria of subjective tinnitus included the following: (I) unilateral or bilateral non pulsatile sound (sustainable or non-sustainable); (II) no abnormalities of hearing structures, including the auditory conduction pathway, inner ear hearing organs, auditory nerve, temporal lobe and brain parenchyma, found by imaging; (III) no causes of objective tinnitus resulting from ear trauma, vascular abnormalities, new organisms, etc. (1,2).

Diagnostic criteria of dominant drainage and high jugular bulb
Dominant drainage of transverse-sigmoid sinus is defined as the transverse sinus on one side, and the diameter of sigmoid sinus is more than 1.5 times that of the opposite side (17). High jugular bulb is defined as the basal rotation of the jugular bulb up to the ipsilateral cochlea (18) (*Figure S1*).

Hemodynamic analysis

CVI-42 has been used to post process the 4D Flow MRI data of all participants, and the specific processing process was as follows. First, the whole processing procedure was based on the small vessel algorithm provided by the software developer to analyze the data. After importing the image data into CVI, the software automatically detected the range of blood flow and performed preprocessing. The software used the offset correction and phase unwrapping function to further optimize the accuracy of blood flow region detection. Secondly, the vessels of interest were segmented and outlined. The vascular segment in this study was sinus confluence to transverse sinus to sigmoid sinus to jugular bulb to internal jugular vein. After the segmentation of vessels, in order to ensure the accuracy of blood flow measurements, the centerlines of blood vessels of interest were further tracked. Using the vessel centerline tracking function of the software, we respectively selected the sinus confluence and internal jugular vein as the start and end points of the centerline. After automatic tracking, we conducted careful inspection and correction to ensure the reliability of the centerline. Thirdly, hemodynamic analysis was performed. At this time, the software showed the segmented vessels' hemodynamic features, including the morphologies of the vessels of interest and the internal blood flow. The visualization of the streamline could help clarify the accuracy of blood flow direction setting. Blood flow abnormalities could be identified according to the changes of streamline color and shape.

Results

Hemodynamic abnormalities in the venous sinus of patients with VPT

There was no significant difference in the TV of the six planes among the three groups, but there were significant differences in the PV and MWSS of the six planes among the three groups (*Table S1*).

Relationship among hemodynamic factors, bone dehiscence, and severity of tinnitus

Plane 3 with the largest variability of blood flow was selected as the appropriate measurement plane to explore the relationship between hemodynamic parameters and the BD in patients with VPT. The TV (r=0.31, P=0.028), PV (r=0.62, P<0.001), MWSS (r=0.49, P<0.001), and MEL (r=0.54, P<0.001) were positively related to the size of BD as shown in *Figures S2,S3*. THI scale was used to evaluate the severity of tinnitus symptoms in patients with VPT. The TV (r=0.38, P=0.007), PV (r=0.63, P<0.001), MWSS (r=0.36, P=0.010), and MEL (r=0.57, P<0.001) on plane 3 were positively correlated with the THI scores. The size of BD in patients with VPT was also positively correlated with the THI score (r=0.47, P=0.002) (as shown in *Figures S2,S4*).

In addition, the results showed that there were no statistically significant correlation between THI and TV (r=0.320, P=0.074), PV (r=−0.058, P=0.753), MWSS (r=0.009, P=0.960), and MEL (r=−0.108, P=0.556) (as shown in *Figure S5*).

The blue band shows the relationship between bone dehiscence and hemodynamics. The PV, MWSS, and MEL were positively correlated with the size of BD. The correlation between the PV and the size of BD was the strongest. The correlation between the TV and the size of BD was the weakest. The pink band shows the relationship between the severity of tinnitus, hemodynamics, and bone dehiscence, the correlation between the PV and THI was the strongest. The correlation between the MWSS and THI was the weakest.

The effect of BD on PT severity is mediated by hemodynamic factors

The MEL and PV showed complete mediation effects between the effect of BD and THI, as shown in *Figure 5A,5B* and *Table S2*. However, when the TV and MWSS were used as mediation variables, the model was invalid (*Figure S6*).

The BD a complete mediation effect between MWSS and THI, as shown in *Figure 5C* and *Table S3*. However, no significant mediation effect existed between the TV, PV, and THI when the BD was used as a mediation variable (*Figure S7*).
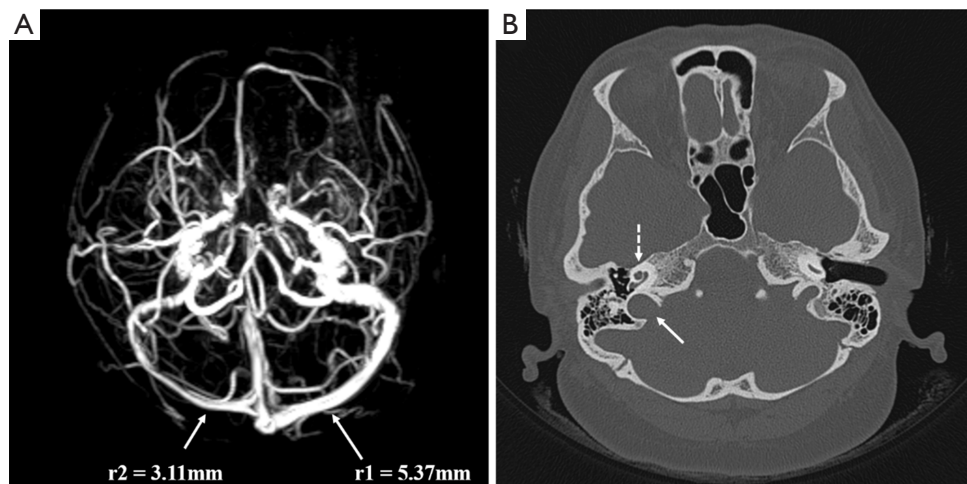

Figure S1 Diagnostic criteria of dominant drainage and high jugular bull. Dominant drainage was defined as the diameter of the vein on the dominant side was 1.5 times greater than that on the contralateral side. The high jugular bull was defined as the level of the jugular bulb reaching the bottom of cochlea on the same side.
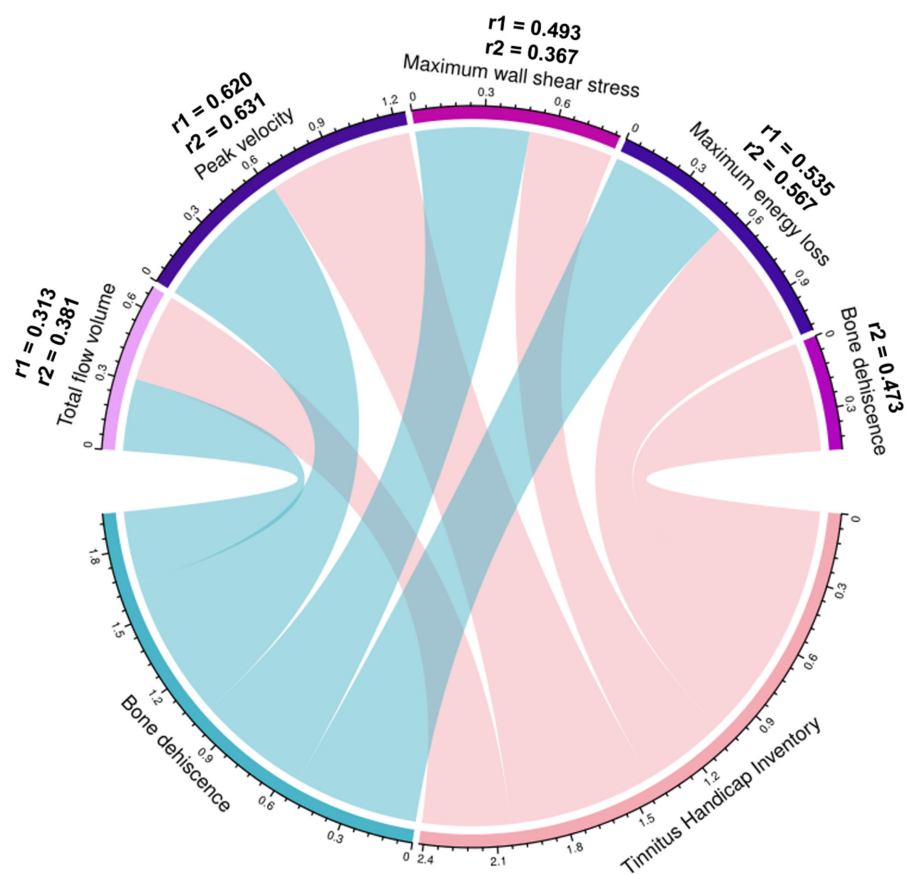
Figure S2 Correlations between the bone dehiscence, hemodynamic parameters, and severity of tinnitus in patients with VPT. VPT, venous pulsatile tinnitus.
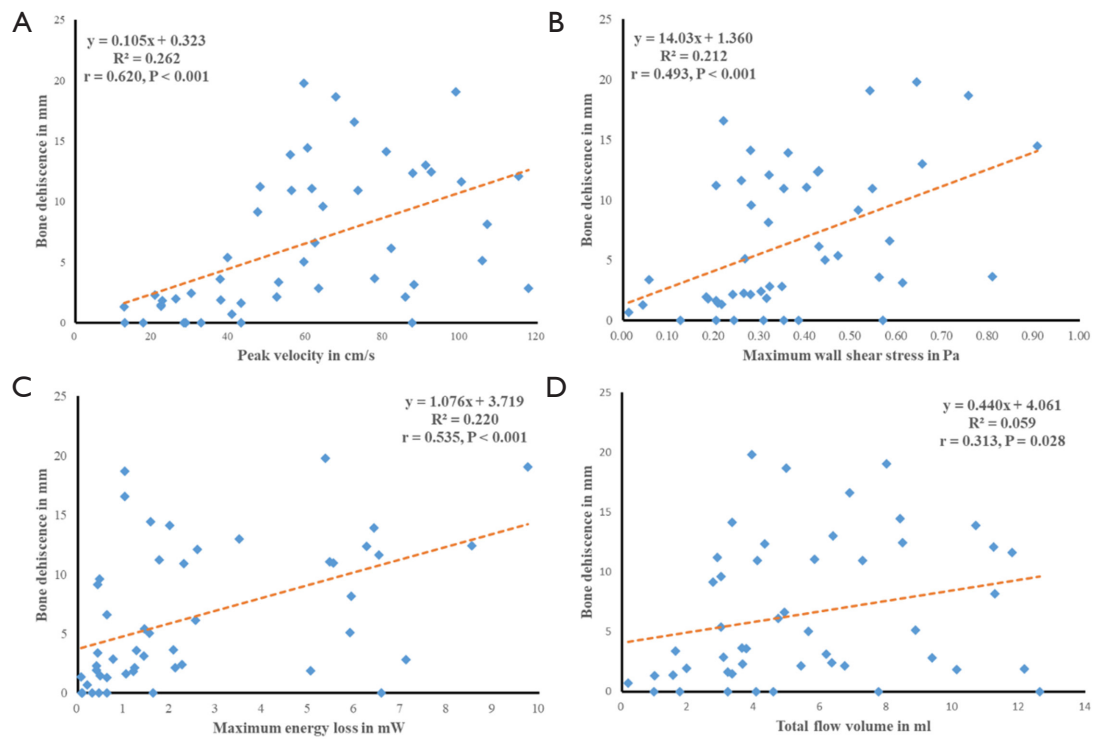
Figure S3 Correlations between bone dehiscence and hemodynamics in PT patients. PV, MWSS and MEL were positively correlated with the size of bone dehiscence. PT, pulsatile tinnitus; PV, peak velocity; MWSS, maximum wall shear stress; MEL, maximum energy loss.
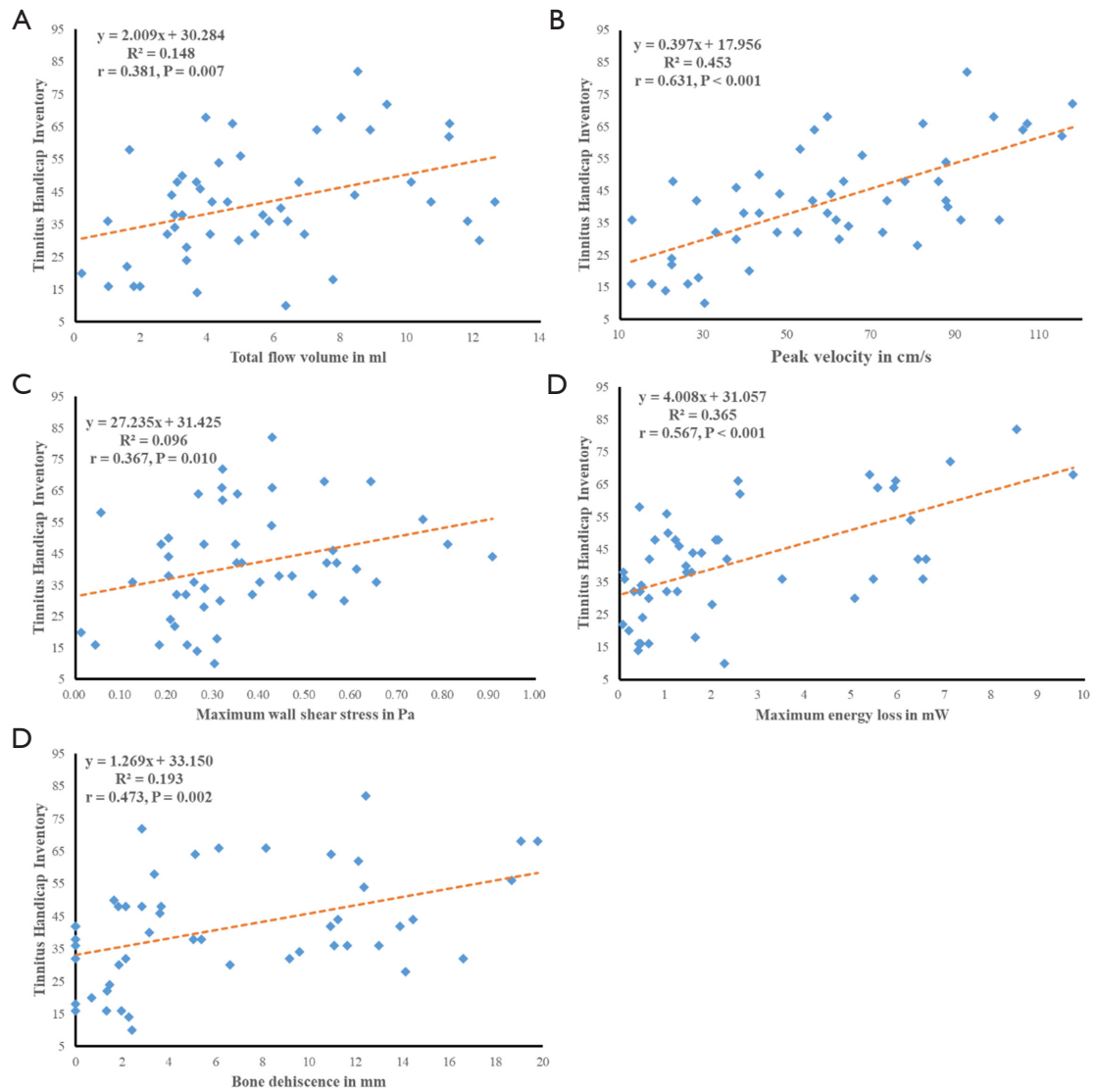
Figure S4 Associations of Tinnitus Handicap Inventory score with hemodynamics and bone dehiscence in PT patients. TV, PV, MWSS and MEL were positively correlated with Tinnitus Handicap Inventory score. The size of bone dehiscence was positively correlated with Tinnitus Handicap Inventory score. PT, pulsatile tinnitus; TV, total blood flow volume; PV, peak velocity; MWSS, maximum wall shear stress; MEL, maximum energy loss.
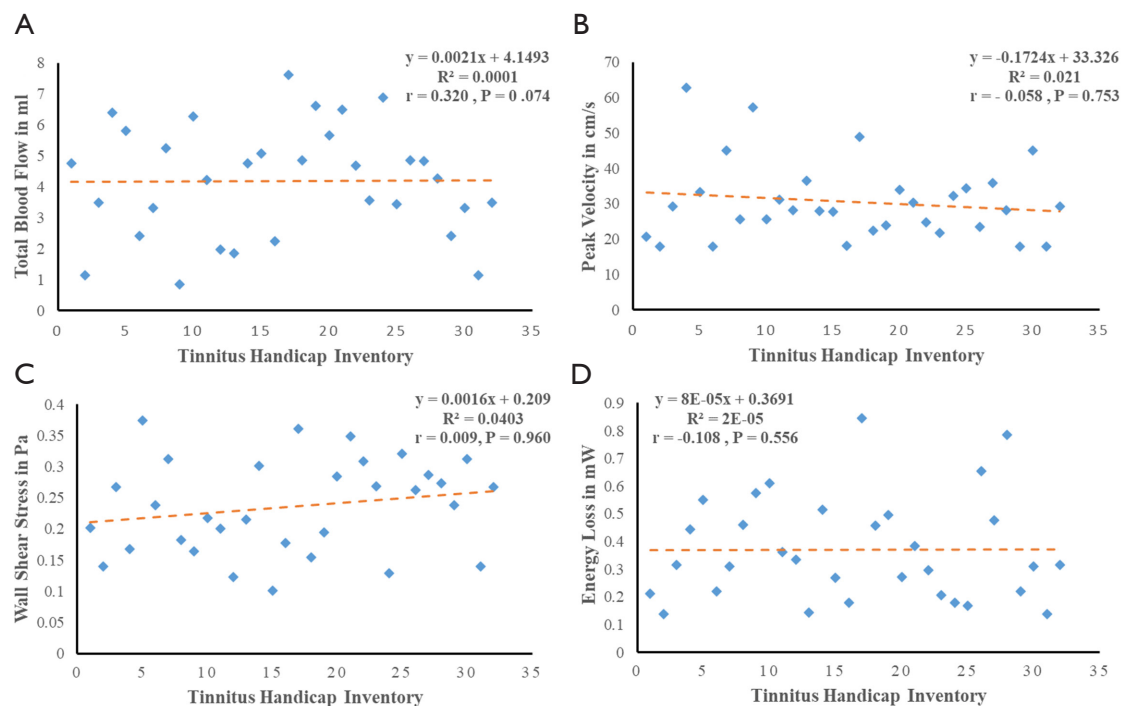
Figure S5 Associations of Tinnitus Handicap Inventory score with hemodynamics and bone dehiscence in ST patients. TV, PV, MWSS and MEL have no obvious correlation with Tinnitus Handicap Inventory score. ST, subjective tinnitus; TV, total blood flow volume; PV, peak velocity; MWSS, maximum wall shear stress; MEL, maximum energy loss.
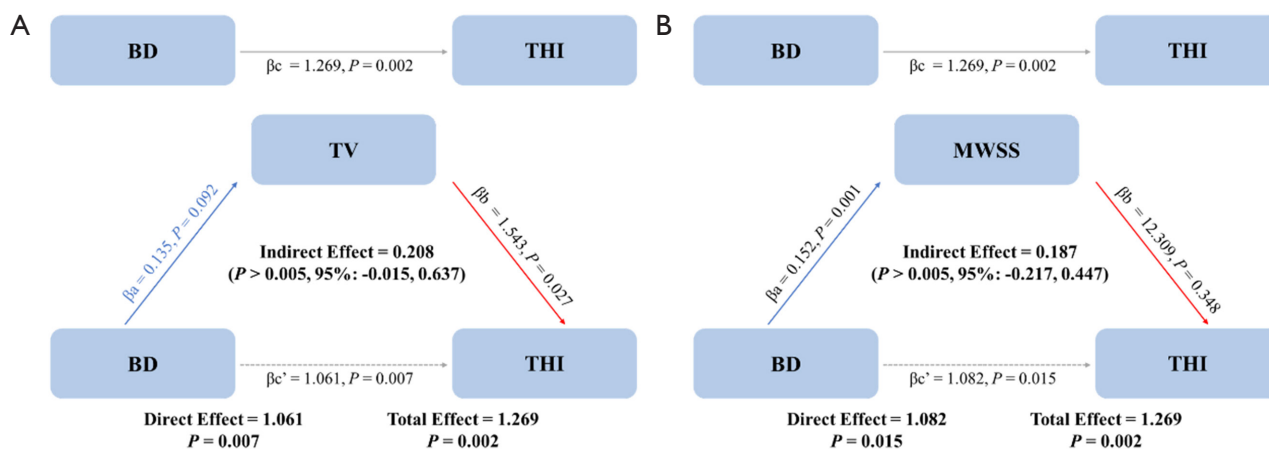

Figure S6 Two non-significant mediation analysis models for hemodynamic parameters in regulating the relationship between BD and THI. BD, bone dehiscence; THI, Tinnitus Handicap Inventory; TV, total blood flow volume; MWSS, maximum wall shear stress.
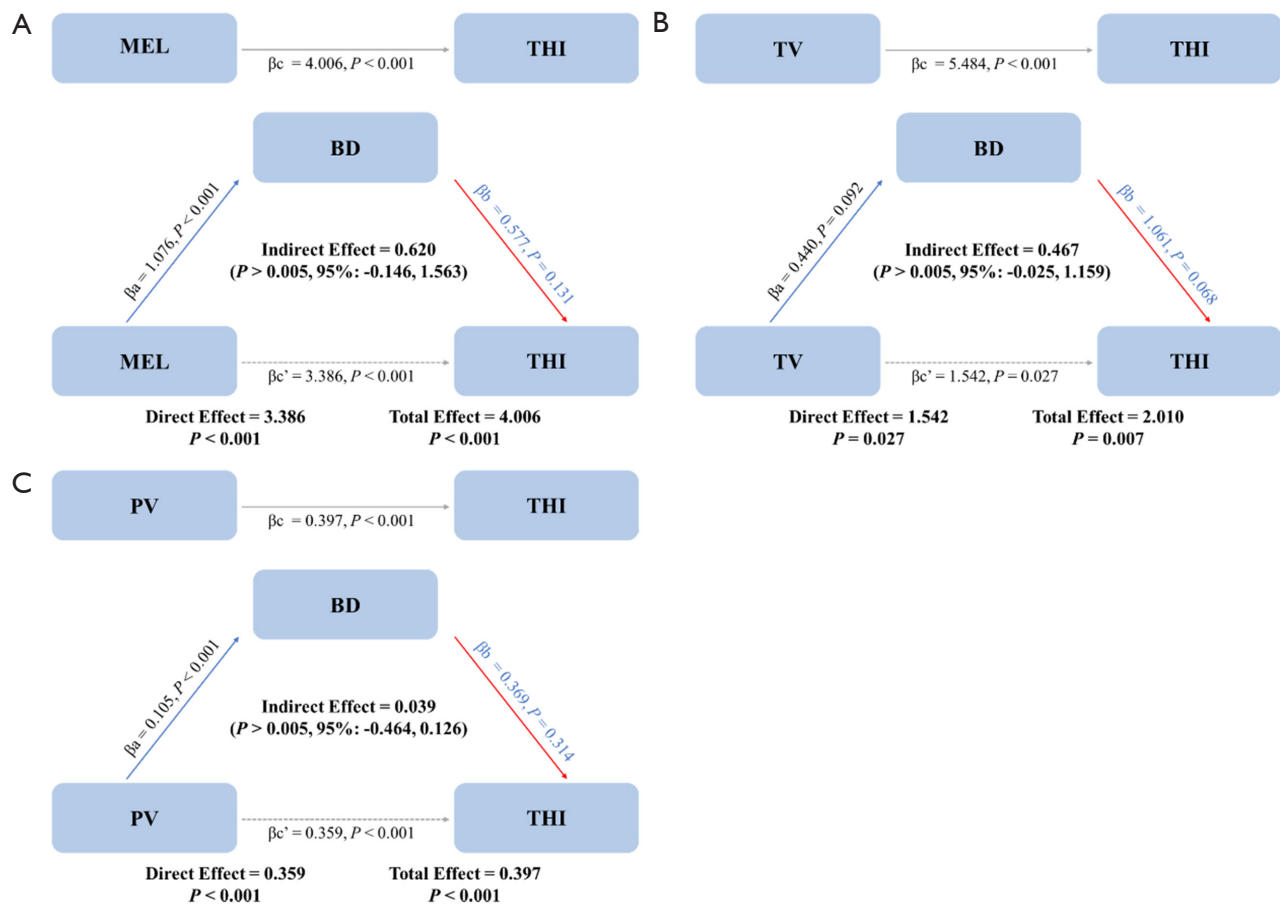
Figure S7 Non-significant mediation analysis models for BD in regulating the relationship between hemodynamics and THI. MEL, maximum energy loss; THI, Tinnitus Handicap Inventory; BD, bone dehiscence; TV, total blood flow volume; PV, peak velocity.

Table S1 Hemodynamic differences in the different planes of transverse-sigmoid sinus in three groups

	Plane 1	Plane 2	Plane 3	Plane 4	Plane 5	Plane 6	F value	P value
VPT								
TV (mL)	4.52 (2.73–6.63)	4.55 (2.47–6.59)	4.73 (2.99–7.87)	4.72 (3.15–7.10)	4.76 (2.47–6.63)	3.29 (2.11–5.29)	10.079	0.073
PV (cm/s)	25.80 (20.77–39.25)	40.68 (29.17–63.48)	59.27 (35.11–83.91)	44.34 (35.23–62.30)	38.56 (34.17–49.22)	26.95 (19.28–30.81)	71.204	<0.001[‡]
MWSS (Pa)	0.23 (0.19–0.30)	0.51 (0.28–0.73)	0.32 (0.24–0.49)	0.38 (0.27–0.44)	0.28 (0.23–0.38)	0.21 (0.16–0.28)	66.589	<0.001[‡]
MEL (mW)	1.55 (0.56–5.21)	–	–	–	–			
HC								
TV (mL)	4.44 (2.88–5.60)	4.15 (2.93–5.11)	3.94 (2.81–5.98)	3.92 (2.80–5.11)	4.10 (3.25–5.72)	3.12 (2.35–5.26)	8.415	0.135
PV (cm/s)	24.47 (19.49–34.58)	31.73 (22.44–38.91)	25.41 (20.78–33.60)	25.78 (21.80–33.94)	28.75 (24.76–35.53)	24.82 (21.27–28.56)	16.365	0.006[†]
MWSS (Pa)	0.25 (0.10–0.31)	0.40 (0.32–0.51)	0.23 (0.19–0.27)	0.28 (0.24–0.32)	0.29 (0.25–0.34)	0.21 (0.17–0.25)	89.742	<0.001[‡]
MEL (mW)	0.30 (0.67–1.20)	–	–	–	–			
ST								
TV (mL)	4.81 (3.63–5.97)	4.15 (2.31–5.61)	4.50 (2.64–5.56)	4.20 (3.05–5.78)	4.53 (3.46–6.21)	3.58 (2.60–4.65)	8.098	0.151
PV (cm/s)	25.60 (20.43–30.89)	29.25 (23.91–35.00)	28.20 (22.63–34.28)	26.02 (22.94–32.67)	32.58 (28.62–40.54)	35.02 (21.24–31.10)	20.913	0.001[†]
MWSS (Pa)	0.25 (0.22–0.31)	0.43 (0.34–0.52)	0.27 (0.20–0.34)	0.32 (0.28–0.36)	0.32 (0.26–0.38)	0.25 (0.22–0.30)	36.473	<0.001[‡]
MEL (mW)	0.41 (0.29–0.68)	–	–	–	–			

[†], $P<0.05$; [‡], $P<0.001$. VPT, venous pulsatile tinnitus; TV, total blood flow volume; PV, peak velocity; MWSS, maximum wall shear stress; MEL, maximum energy loss; HC, healthy control; ST, subjective tinnitus.

Table S2 Mediating efficacy with hemodynamic parameters used as mediating variables

Mediating factor	Effect	Boot SE	T	P	95% confidence interval	
					LLCI	ULCI
MEL						
Total effect	1.269	0.379	3.350	0.002	0.507	2.031
Direct effect	0.577	0.375	1.538	0.131	−0.178	1.331
Indirect effect	0.692	0.300	–	–	0.201	1.377
PV						
Total effect	1.269	0.379	3.350	0.002	0.507	2.031
Direct effect	0.369	0.363	1.018	0.314	−0.361	1.100
Indirect effect	0.899	0.295	–	–	0.406	1.582

SE, standard error; LLCI, lower limit of the confidence interval; ULCI, upper limit of the confidence interval; MEL, maximum energy loss; PV, peak velocity.

Table S3 Mediating efficacy with bone dehiscence used as an independent variable

Mediating factor	Effect	Boot SE	T	P	95% confidence interval	
					LLCI	ULCI
BD						
Total effect	27.489	12.170	2.259	0.029	3.008	51.971
Direct effect	12.309	12.993	0.947	0.348	−13.844	38.462
Indirect effect	15.181	8.417	–	–	3.448	35.493

SE, standard error; LLCI, lower limit of the confidence interval; ULCI, upper limit of the confidence interval; BD, bone dehiscence.